Spatially and Temporally Resolved Thermal Imaging of Cyclically Heated Interconnects by Use of Scanning Thermal Microscopy

NICHOLAS BARBOSA III* AND ANDREW J. SLIFKA
Materials Reliability Division, Materials Science and Engineering Laboratory, National Institute of Standards and Technology, Boulder, Colorado 80305

KEY WORDS calibration; interconnect; cyclic joule heating; temperature distribution; temporal; thermal cycling; scanning thermal microscope; Wollaston probe; SThM

ABSTRACT A scanning thermal microscope with a Wollaston probe was used to investigate the spatial distribution and temporal variation of temperature in interconnect structures subjected to thermal cycling. The probe, utilized in passive temperature sensing mode, was calibrated from 20°C to 200°C using a single-layer aluminum microdevice. Spatial measurements were performed on nonpassivated aluminum interconnects sinusoidally heated by a 6 MA/cm^2 current at 200 Hz. The interconnects were determined to have temperatures that decreased with position from a maximum located at the center of both the interconnect length and width. Time-resolved temperature measurements were performed on the same structures sinusoidally heated by a 6 MA/cm^2 current at 2 Hz. Both the peak-cycle temperature and average-cycle temperature were found to decrease with increasing distance from the center of the width of the interconnects. *Microsc. Res. Tech. 71:579–584, 2008.* Published 2008 Wiley-Liss, Inc.†

INTRODUCTION

Many micro- and nano-devices receiving recent attention are either electrically actuated or have components that carry current. The design of reliable devices at these scales requires special consideration to thermal management issues in order to accommodate joule heating. Temperature fluctuations caused by heating have the potential to affect device stress states and ultimately device lifetimes. Currently, few tools exist to measure temperature at this scale and none have been demonstrated for both the investigation of spatial- and time-resolved temperature properties of devices at the micro- and nano-levels. The purpose of this study is to investigate the use of scanning thermal microscopy (SThM) using a Wollaston probe in passive temperature sensing mode as a technique to directly measure the spatial- and time-resolved temperature profile of electrical interconnects during cyclic joule heating.

SThM comprises a group of techniques that provide near-field micrometer- and nanometer-scale thermal-property measurements. SThM techniques can be grouped into three categories (Majumdar, 1999). Thermovoltage-based techniques typically utilize micro- and nano-scale thermocouples integrated into atomic force microscope (AFM) cantilever tips (Majumdar et al., 1995; Williams and Wickramasinghe, 1986). Thermal expansion techniques utilize an external heat source to manipulate specimen temperature, and sample dimensions are measured with an AFM (Barnes et al., 1994; Igeta et al., 1999). Electrical resistance techniques utilize the current-voltage response of a platinum AFM tip as a function of temperature to measure local conductivity or temperature variations (Buck et al., 1997; Dinwiddie et al., 1994; Lefevre et al., 2003).

SThM temperature measurements are most often performed through thermovoltage-based and resistance-based techniques. Thermal expansion techniques are typically used for measuring the local thermal expansion properties of a material, but suffer from convolution of thermal conductivity and diffusivity mechanisms. Thermovoltage-based techniques are performed with integrated thermocouple tips produced through microfabrication procedures and are proficient at performing fine-scale spatial measurements from regions as small as 50 nm (Shi et al., 2000). Interpretation of the data from thermovoltage techniques can be difficult because of the multiple heat transfer mechanisms active at the size scale of interest, including solid–solid conduction, radiation, liquid-meniscus conduction, and convective transfer. Electrical resistance techniques, including the technique described in this work, also suffer from similar interpretation difficulties, but have the advantage of multiple operational modes (Fiege et al., 1999; Lefevre et al., 2003; Majumdar, 1999; Pollock and Hammiche, 2001; Volz et al., 2006), allowing for temperature, conductivity, and calorimetric measurements. In addition, resistance techniques have a significant thermal resolution advantage over thermo-

*Correspondence to: Nicholas Barbosa III, Materials Reliability Division, Materials Science and Engineering Laboratory, National Institute of Standards and Technology, 325 Broadway, MS853, Boulder, CO 80305.
E-mail: barbosa@boulder.nist.gov

Received 30 November 2006; accepted in revised form 7 February 2008

DOI 10.1002/jemt.20589

Published online 5 May 2008 in Wiley InterScience (www.interscience.wiley.com).

voltage-based techniques; resistance thermometers operate at $\pm 0.1^{\circ}$C where thermocouples typically have a maximum precision of $\pm 0.5^{\circ}$C (Holman, 1994).

The majority of resistance SThM tips are Wollaston probes. Microfabricated tips, however, are also available (Majumdar, 1999). Wollaston probe tips are both more robust and less sensitive to spatial temperature variations when compared to the micro-fabricated resistive tips and typically consists of a coaxial wire with a 5-μm-diameter Pt or Pt-alloy core sheathed by a 75-μm-diameter Ag layer. The coaxial wire is bent into a "V" shape and the Ag is removed from ~100 μm of wire length on either side of the apex, exposing the Pt core wire used for the resistance measurement. A mirror is mounted onto the Ag-coated area of the probe for AFM displacement feedback. In contrast to the relatively large wire diameter, the effective contact area of Wollaston probes has been shown to be in the range of 30–300 nm, and although we did not measure the spatial resolution in this work, previously it has been shown to be better than 400 nm (Fiege et al., 1997; Pylkki et al., 1994). Tips are hand-made and so variation in resolution is not uncommon.

Temperature measurement is typically performed in the passive mode, where a current low enough to preclude measurable joule heating in the tip is passed through the wire and the voltage is monitored during scanning. Knowledge of the current and voltages in the wire allows for the resistance of the wire to be calculated. A conventional Wheatstone bridge operating in unbalanced mode is utilized to measure voltage changes in the sensor. Changes in wire resistance are then related to temperature through a calibration curve.

As to the knowledge of the authors, three methods have been reported for calibrating SThM tips: ambient temperature variation (Buck et al., 1997) for calibration of Wollaston probe tips, bulk substrate variation (Majumdar et al., 1995) for thermocouple type tips, and localized temperature variation (Shi and Majumdar, 2001) for thermocouple type tips. In the case of thermocouple tip calibration, the heat sensing volume is determined by the thermocouple junction size, minimizing the impact of the relative size difference between the heat source the tip. Even so, the heat flow through the single crystal silicon cantilever may be affected by the geometry of the cantilever (Shi and Majumdar, 2001) and should be considered. For Wollaston probe tips, the effect of the heat source (geometry and temperature range) on the tip calibration is more significant.

Typically, the dependence of resistance on temperature is measured with a sample of a known and fixed geometry. The location of the voltage measurement points defines the sensor size and thus the resistance is measured over a fixed volume, neglecting changes due to thermal expansion. In the case of the Wollaston probe, the voltage measurement points are located far from the tip, making the geometry of the sensing element poorly defined. Two heat sources of different sizes have the potential to generate different measured resistance values in the Wollaston probe even though the contact area between the sample and probe may not vary significantly. Since the heat conductance through the air surrounding the probe plays a significant role in the overall heat transfer of the system (Volz et al., 2006), a larger heat source will affect a larger volume of the probe, producing an overall resistance change dependent on both temperature (desired) and amount of probe volume heated (undesired). Special care must be employed to ensure that the calibration heat source is similar in size and geometry to the sample in question ensuring that the calibrated sensing volume in the tip remains constant.

In this work, a Wollaston probe SThM operating in the passive mode was used to qualify an electrical approach to measuring mechanical properties and estimating reliability in thin films. The new measurement technique, described elsewhere (Keller et al., 2002; Mönig et al., 2004), imposes strains in patterned metal lines adhered to Si substrates through mismatched coefficients of thermal expansion between the lines and the substrate. Knowledge of the spatial- and time-resolved thermal state of the test line provides information about the strain distribution in the specimens, a key factor in the test method. The strain change $\Delta\varepsilon$ in the specimen is related to the temperature change ΔT through the mismatch in coefficient of thermal expansion, $\Delta\alpha$:

$$\Delta\varepsilon = \Delta\alpha \cdot \Delta T. \tag{1}$$

This relation also holds on a local scale. Global changes in line temperature are measured through changes in line resistivity. This method of temperature measurement assumes Matthiessen's rule and relies on the relation:

$$R(T) = R_{\circ} + \Delta T \cdot \frac{\mathrm{d}\rho}{\mathrm{d}T} \cdot \frac{L}{A} \tag{2}$$

where $R(T)$ is the resistance at temperature T, $R_{\circ}$ is the resistance at the reference temperature, $\mathrm{d}\rho/\mathrm{d}T$ is the change in resistivity with temperature, L is the line length, and A is the line cross-sectional area. Finite element analysis (FEA) (Keller et al., 2002) and observations of damage development during testing suggest that temperature in the lines is not uniform. The line resistivity method of temperature measurement does not capture local temperature variation, and hence, we seek local measurements of temperature as a function of position to better characterize the strain state induced during testing.

The SThM was used to directly measure temperature under actual test conditions. Measurements on interconnects 1–10 μm wide undergoing thermal cycling at 200 Hz require submicrometer resolution and sampling frequencies significantly higher than 200 Hz to sufficiently characterize the strain state of the interconnects. Wollaston SThM probes have been shown to be capable of submicrometer spatial resolutions (Fiege et al., 1997; Pylkki et al., 1994) and have a thermal response time of less than of 200 μs (Ezzahri et al., 2005) providing the potential for data collection at frequencies greater than 1 kHz. To our knowledge, there are currently no alternate techniques that have been shown to be capable of providing time-resolved thermal information at this spatial resolution or timescale.

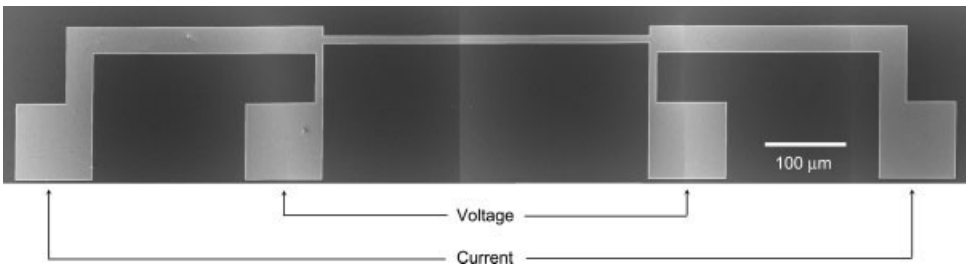

Fig. 1. A plan-view scanning electron microscope (SEM) image of the 500-nm-thick aluminum interconnect test structure investigated with the SThM. The narrow gauge section between the voltage taps is the area of interest. The two voltage taps and the two current taps allow for simultaneous heating and measurement of resistance through four-point resistance measurements.

EXPERIMENTAL PROCEDURES

Interconnects were single-level, nonpassivated structures fabricated by depositing aluminum films on silicon wafers through electron-beam evaporation. Pattern definition was accomplished by lift-off lithography. Interconnects were 400 μm long, 8 μm wide, and 0.5 μm thick. Each interconnect was connected to two bond pads on each end to enable current cycling as well as four-point resistance measurements (Fig. 1). Multiple structures were patterned on a single chip and multiple chips were fabricated on a single wafer. After separating a chip from the wafer, we mounted it on a ceramic package with Ag paste for thermal contact. Electrical connections were made through wire bonding. Interconnect thermal cycling was performed under current control while voltage was monitored. Data acquisition and control were performed through custom software, a computer card, and a current calibrator. Further details regarding interconnect thermal cycling may be found elsewhere (Barbosa et al., 2007).

Prior to temperature measurement in passive mode, calibration of the Wollaston probe was accomplished over the range 20°C to 200°C through the use of a single-layer aluminum microdevice. The calibration device consisted of both a resistive heater and a four-point resistance sensor shown in Figure 2. The device was designed to maintain a constant sensor temperature between the sensor voltage taps as previous FEA work and observations have shown that line temperatures vary at the ends of some interconnect structures (Keller et al., 2002). The small resistive heater and sensor provided a calibration source of comparable size and power output to the structure of interest, which as previously discussed is important when using a Wollaston probe at high temperatures.

Four steps were used to ensure that the calibration device worked as designed. First, the calibration device sensor was checked for uniform temperature during resistive heating. The uncalibrated SThM was used to detect any measurable voltage variation (indicating temperature variation) between the voltage taps shown in Figure 2. Second, the absolute temperature of the device sensor was calibrated by measuring the four-point resistance as a function of chip temperature without resistive heating. Instead, the sensor temperature was controlled with a hotplate, which heated the entire calibration device while the temperature was measured with a conventional thermocouple bonded with Ag paste to the chip surface. Third, the SThM and tip were calibrated by locating the tip on the sensor and varying the sensor temperature though the resistive on-chip heater. In this method, a linear calibration curve from 20°C to 200°C was determined for the SThM tip. Temperature sensitivity was determined to be within ±0.5°C. Finally, the first step was repeated with a calibrated tip. Temperature variation across the sensor was found to vary less than the sensitivity of the tip, or less than 0.5°C. Calibration to a higher temperature is possible by changing the resistive heater material from aluminum to a higher melting point material.

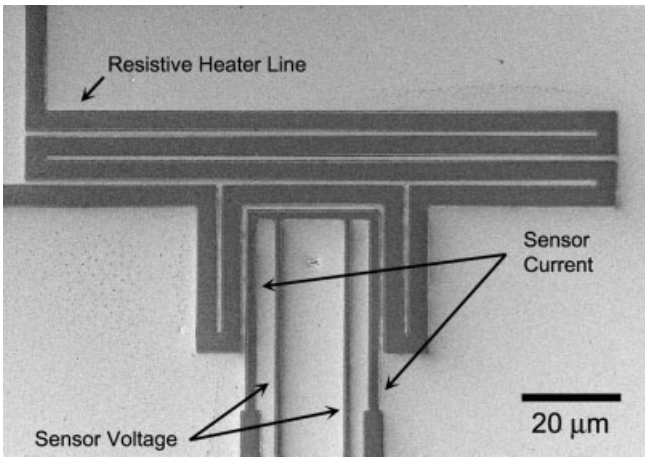

Fig. 2. An SEM image of the structure used to calibrate the SThM tip. Both the resistive heater and temperature sensor were fabricated from 300-nm-thick aluminum, which allowed for easy fabrication, but limited the maximum operating temperature to several hundred degrees Celsius. The design ensured that the calibration area, located on the sensor structure between the sensor voltage taps, was at a uniform temperature throughout the structure.

After calibration, both spatial and temporal information were obtained with the SThM through two types of experiments. To obtain spatial temperature information, the microscope was operated similarly to a conventional AFM, but in addition to topographic information, temperature information was obtained from the Wollaston probe during imaging of the scan area. For these experiments, the SThM was operated at a scan size of 50 μm × 50 μm and a frequency of 1 Hz. The

interconnects were heated at 200 Hz and a current density of 6 MA/cm^2. The interconnect heating frequency is typical of tests performed with this type of interconnect (Barbosa et al., 2007) and the current density provided sufficient interconnect heating without causing specimen damage. After thermal cycling was initiated, the system was allowed to reach thermal equilibrium prior to SThM measurement. Equilibrium was determined through changes in four-point resistance measurements.

Temporal information was obtained by placing the microscope tip at locations across the width of the interconnect and capturing temperature data at each location. The tip was not scanned during the acquisition of temporal data. Interconnects were again heated with a current density of 6 MA/cm^2, but the heating frequency was decreased to 2 Hz because of limitations imposed by instrument specific data collection electronics. A time delay was also implemented prior to temporal measurements to allow for the system to reach thermal equilibrium.

RESULTS AND DISCUSSION
Spatially Resolved Thermal Imaging

Spatial SThM imaging during thermal cycling at 200 Hz was performed on a 400-μm-long, 8-μm-wide, and 0.5-μm-thick aluminum interconnect. Figure 3(a) is a schematic showing the location of the 50 μm × 50 μm scan on the interconnect. The scan included part of the line section as well as part of the bond pad area. The dashed lines in Figure 3(a) show the locations from where the line scans in shown Figure 3(b) were extracted to obtain temperature profiles along the line width and line length. The line profiles in Figure 3(b) are the result of posttest processing that will be discussed later. As a reference, the edges of the interconnect are shown as vertical lines in Figure 3(b).

Figure 4 shows line one (L1) data from Figure 3 with only minimal signal processing; it also shows the results of the application of three separate moving average filters. Only high-frequency noise causing signal saturation attributed to topographic variation was removed from the "no filter" data in the figure. Four distinct features are present in the L1 line scan shown in Figure 4(a): an average temperature increase near the midpoint of the width of the interconnect, a cyclic temperature fluctuation along the line scan, prominent temperature spikes such as the downward spike located at a distance of ~25 μm, and a section of data missing from between ~18 and 20 μm.

The average temperature change across the width and length of the interconnect was extracted from the raw data through several processing steps. First, as previously mentioned, the signal irregularities causing saturation were removed, leaving the data as seen in Figure 4. This was the cause of the data gaps in L1 in both Figures 3(b) and 4(a). Local thermal conductivity variation as well as tip-sample geometry interactions were the cause of these large signal variations (Fiege et al., 1997).

Cyclic temperature fluctuations along the line scan, a result of the relationship between the interconnect heating frequency and the SThM scan frequency, were then removed. When the thermal-cycle frequency is much greater then the scan frequency, cyclic noise will not be present in the data because the SThM experiences several temperature cycles while dwelling at each pixel location. As the frequencies converge, and cyclic data is superimposed on temperature-position data, averaging techniques can be used to obtain the average line temperature at a location. In this work, the cyclic temperature variation was smoothed through the use of a 30-point moving average filter. Figure 4(a) shows an 8 point moving average, a 30 point moving average, and a 50 point moving average. Figure 4(b) shows that while all of the filters capture the same general trends, an 8 point moving average, selected for the relative number of SThM data points scanned during one temperature cycle, does not remove all of the cyclic noise. While the choice of a filter type depends on the frequencies involved, the 30 point moving average clearly captures the average data trend without significant information loss and is suitable for this work.

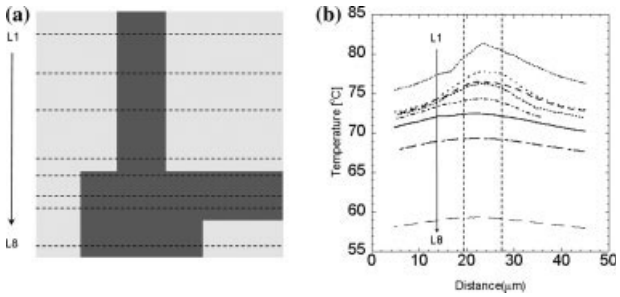

Fig. 3. **a**: A schematic AFM scan of an interconnect similar to the one shown in Figure 1. Note that the schematic is rotated 90° counterclockwise. The lightly shaded region shows the extent of the Edescan area, the darkly shaded region shows the interconnect position, and the dashed lines show locations where eight lines of data were extracted. **b**: Extracted data after application of a 30-point moving average filter and removal of high-frequency, topographic noise. The edges of the gauge section of the interconnect are indicated by vertical lines.

From the spatial scans it was clear that temperature in the interconnect was not uniform, but in fact systematically varied with position. The maximum temperature determined from the scan area using the 30 point moving average was 81.5°C and was found toward the center of the length of the line and at the middle of the width of the line. This value decreased to 74°C at the edge of the bond-pad area. The temperature continued to decrease to less than 60°C at a location within the bond-pad area. Temperatures also decreased with distance away from the middle of the width of the line by 1–2°C for L1. An additional 2°C decrease was measured at a distance of 10 μm from the center of the line width, within the silicon substrate. This trend was also present in L2 through L8, but the line profiles were more diffuse near and in the bond-pad area. The decrease in temperature along the width of the line is due to heat flow from the line to the substrate. The decrease in temperature along the length of the line is due to the bond-pad area acting as a heat sink in addition to the line-substrate heat flow. Both results were in agreement with FEA results (Mönig et al., 2004).

In addition, no scans showed a distinct temperature change as the SThM tip moved from scanning on the surface of the interconnect at the line edge to scanning

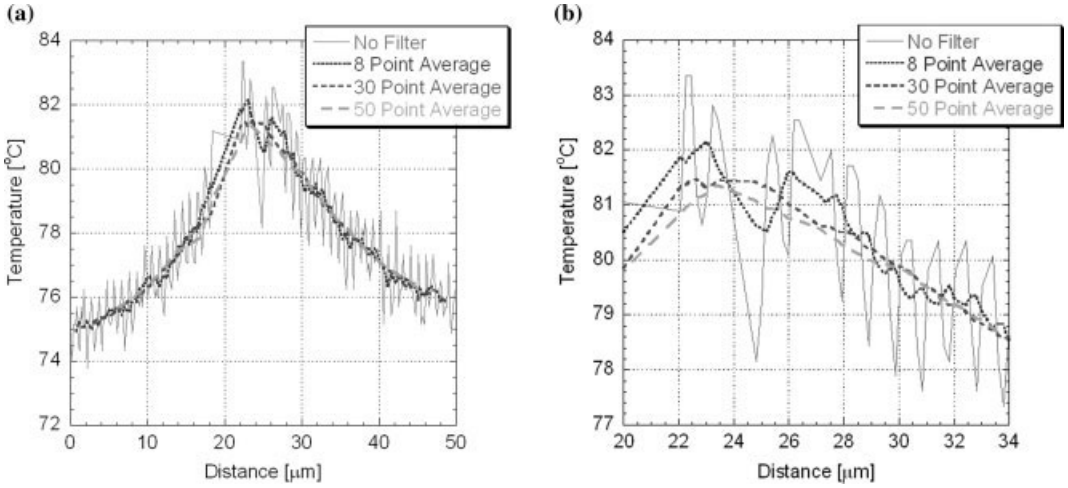

Fig. 4. **a**: Raw data from scan line one (L1) of Figure 3(b) with 8, 30, and 50 point moving averages applied. **b**: An enlargement of the same data detailing the ability of the filters to smooth the data.

on the nearby substrate. The diffuse thermal profiles across the line edge are consistent with work on electromigration (Buck et al., 1997) and are due to the high thermal conductivity of the silicon substrate, 124 W/(m K) (Lide, 1993) and the intimate contact between the interconnect and substrate, allowing for rapid heat flow from the interconnect source to the substrate thermal reservoir.

Time-Resolved Thermal Imaging

Time-resolved imaging was performed on an interconnect with the same dimensions as the one described in the previous section. By maintaining a constant SThM tip position during thermal cycling, changes in temperature with time were recorded. Figure 5 shows four waveforms obtained at four locations across the width of the interconnect. The timescales of individual waveforms were adjusted to be in phase for comparison purposes. The waveforms in Figure 5 were obtained while a 6 MA/cm^2 sinusoidal rms signal was applied to the interconnect at a frequency of 2 Hz. Waveforms in Figure 5 consist of 1 s pieces of data because of limits imposed by the data collection software. The maximum scan frequency of the SThM is limited by the response time of the Wollaston probe, previously determined to be on the order of 200 μs (Ezzahri et al., 2005).

Sinusoidal functions fitted to the waveforms in Figure 5(b) revealed no deviations from the expected response to sinusoidal excitation at relatively low current densities. The frequency of the sinusoidal temperature cycling was measured to be 2 Hz. Both the temperature amplitude and peak temperature decreased from the center of the line width, to a location 9 μm from the center of the line width. At positions A–C, all located within the aluminum interconnect, the minimum waveform temperatures coincided with one another, but at position D, located on the silicon substrate, the minimum temperature decreased by 1–2°C from the minimum temperature determined at locations A–C. The temperature resolution measured from time-resolved testing results was 0.5°C.

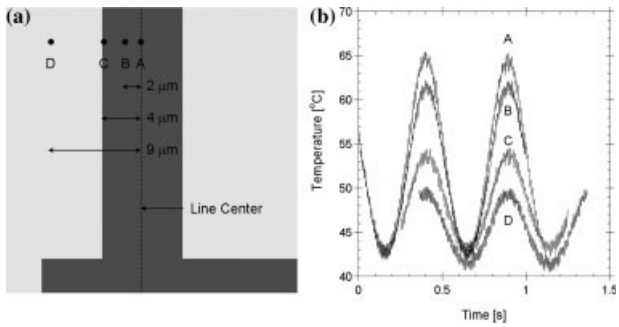

Fig. 5. **a**: Schematic showing the locations of time-resolved SThM line scans across the width of the cyclically heated interconnect. **b**: Four 1-s line scans obtained at the locations denoted in (a) at a scan frequency of 0.5 Hz. The scan lines do not contain a full 2 s of data because the line scan captured only forward trace data, not the data associated with repositioning the tip to the scan start position.

The time-resolved results in Figure 5 were consistent with the spatial measurement results in Figure 3. In both cases, the peak temperature location was at the center of the line width and temperature decreased with increasing distance from the line-width center. Time-resolved imaging yielded more detailed results, which showed that the minimum interconnect temperature did not change across the width of the interconnect, but the minimum cyclic temperature decreased when the SThM tip was located within the silicon substrate. During cycling, joule heating varied between the maximum value, which coincided with the peak of the temperature waveform, and no joule heating, which coincided with the minimum cyclic temperature. At the minimum cycle temperature, the high thermal conductivity of the aluminum, 237 W/(m K) (Lide, 1993), allowed for the rapid redistribution of heat within the interconnect and the low thermal conductivity of the SiO_2 layer, 1.4 W/(m K) (Lide, 1993), acted as a barrier to heat flow through the layer into the silicon substrate. The uniform temperature measured at different locations within the interconnect is due to both mechanisms. The thermally resistive layer was also

responsible for the small temperature decrease in the minimum temperature measured within the silicon substrate near the interconnect.

CONCLUSIONS

SThM using a Wollaston probe operated in passive temperature sensing mode can be used to perform spatially-resolved temperature measurements on interconnects during cyclic heating at 200 Hz. Nonpassivated aluminum interconnects were cyclically heated and found to have nonuniform temperature distributions along their lengths and widths. Maximum temperatures were located at the centers of the width and length of the interconnects. Temperatures decreased toward the edge of the width of the interconnects and toward the end of the gauge length of the interconnects. Time-resolved temperature measurements can be performed to determine local temperature information and have been demonstrated to resolve temperature fluctuations of 2 Hz. Measurement of higher frequencies is limited by device electronics. Time-resolved data obtained at discrete locations indicated that at the frequency and power level investigated, heating was sinusoidal and both peak cycle temperature and average cycle temperature reach a maximum at the center of the width of the interconnects; both values decrease at locations removed from the center of the width of the interconnect. The results of the time-resolved measurements were in agreement with the results of the spatially resolved measurements.

ACKNOWLEDGMENTS

The authors thank the NIST Office of Microelectronics Programs for support. This research was performed while N. Barbosa held a National Research Council Research Associateship at NIST.

REFERENCES

Barbosa N, III, Keller RR, Read DT, Geiss RH, Vinci RP. 2007. Comparison of electrical and microtensile evaluations of mechanical properties of an aluminum film. Metall Mater Trans A 38A:2167.

Barnes JR, Stephenson RS, Woodburn CN, O'shea SJ, Welland ME, Rayment T, Gimzewski JK Gerber C. 1994. A femtojoule calorimeter using micromechanical sensors. Rev Sci Instrum 65:3793–3798.

Buck A, Jones BK Pollock HM. 1997. Temperature and thermal conductivity modes of scanning probe microscopy for electromigration studies. Microelectron Reliab 37:1495–1498.

Dinwiddie RB, Pylkki RJ, West PE. 1994. Thermal conductivity contrast imaging with a scanning thermal microscope. In: Tong T, editor. Thermal conductivity, Vol. 22. Lancaster, PA: Technomic. pp. 668–677.

Ezzahri Y, Lopez LP, Chapuis O, Dilhaire S, Grauby S, Claeys W, Volz S. 2005. Dynamical behavior of the scanning thermal microscope (SThM) thermal resistive probe studied using Si/SiGe. Superlattices Microstruct 38:69–75.

Fiege G, Cramer R, Balk L, Reineke F. 1997. Temperature profiling with highest spatial and temperature resolution by means of scanning thermal microscopy (SThM). In: Proceedings of the 23rd International Symposium for Testing and Failure Analysis (ISTFA '97), pp. 51–56.

Fiege G, Altes A, Heiderhoff R, Balk L. 1999. Quantitative thermal conductivity measurements with nanometre resolution. J Phys D: Appl Phys 32:L13–L17.

Holman JP. 1994. The measurement of temperature. In: J. Corrigan and Eleanor Castellano, editors. Experimental methods for engineers. McGraw-Hill, New York. pp. 324–391.

Igeta M, Inoue T, Varesi J, Majumdar A. 1999. Thermal expansion and temperature measurement in a microscopic scale by using the atomic force microscope. JSME Int J Ser B 42:723–730.

Keller RR, Mönig R, Volkert CA, Arzt E, Schwaiger R, Kraft O. 2002. Interconnect failure due to cyclic loading. AIP Conf Proc 612:119–132.

Lefevre S, Volz S, Saulnier J, Fuentes C, Trannoy N. 2003. Thermal conductivity calibration for hot wire based dc scanning thermal microscopy. Rev Sci Instrum 74:2418–2423.

Lide DR, editor. 1993. Handbook of chemistry and physics. Boca Raton: CRC Press.

Majumdar A. 1999. Scanning thermal microscopy. Annu Rev Mater Sci 29:505–585.

Majumdar A, Lai J, Chandrachood M, Nakabeppu O, Wu Y, Shi Z. 1995. Thermal imaging by atomic force microscopy using thermocouple cantilever probes. Rev Sci Instrum 66:3584–3592.

Mönig R, Keller RR, Volkert CA. 2004. Thermal fatigue testing of thin metal films. Rev Sci Instrum 75:4997–5004.

Pollock H, Hammiche A. 2001. Micro-thermal analysis: Techniques and applications. J Phys D: Appl Phys 34:R23–R53.

Pylkki R, Moyer P, West P. 1994. Scanning near-field optical microscopy and scanning thermal microscopy. Jpn J Appl Phys Part 1 (Regul Pap Short Notes) 33:3785–3790.

Shi L, Majumdar A. 2001. Recent developments in micro and nanoscale thermometry. Microscale Thermophys Eng 5:251–265.

Shi L, Plyasunov S, Bachtold A, Mceuen PL, Majumdar A. 2000. Scanning thermal microscopy of carbon nanotubes using batch-fabricated probes. Appl Phys Lett 77:4295–4297.

Volz S, Lefevre S, Chapuis P. 2006. Nanoscale heat transfer at contact between a hot tip and a substrate. Int J Heat Mass Transfer 49: 251–258.

Williams C, Wickramasinghe H. 1986. Scanning thermal profiler. Appl Phys Lett 49:1587–1589.